

Multiscale Trend Analysis

Ilya Zaliapin ^{*};
Andrei Gabrielov [†] and
Vladimir Keilis-Borok [‡]

May 04, 2003

^{*}Institute of Geophysics and Planetary Physics, University of California, Los Angeles, USA, 90095-1567, and International Institute of Earthquake Prediction Theory and Mathematical Geophysics, Russian Academy of Sciences, Moscow, Russia, E-mail: zal@ess.ucla.edu Phone: +10-310-8256115, Fax: +10-310-2063051, corresponding author.

[†]Departments of Mathematics and Earth and Atmospheric Sciences, Purdue University, IN, USA. E-mail: agabriel@math.purdue.edu

[‡]Institute of Geophysics and Planetary Physics and Department of Earth and Space Sciences, University of California, Los Angeles, USA, and International Institute of Earthquake Prediction Theory and Mathematical Geophysics, Russian Academy of Sciences, Moscow, Russia, E-mail: vkb@ess.ucla.edu

Abstract

We consider the problem of constructing optimal piecewise linear approximations for time series. An optimality criterion is formulated and on its base a computationally effective algorithm is constructed for decomposition of a time series into a hierarchy of trends (local linear approximations) at different scales. The top of the hierarchy is the global linear approximation over the whole observational interval, the bottom is the original time series. Each internal level of the hierarchy corresponds to a piecewise linear approximation of analyzed series. Possible applications of the introduced Multiscale Trend Decomposition (MTD) go far beyond the linear interpolation problem: This paper develops and illustrates methods of self-affine, hierarchical, and correlation analyses of time series based on the MTD.

1 Introduction and Motivation

The motivation for the Multiscale Trend Analysis (MTA) introduced in this paper is to describe and analyze time series in terms of their observed trends (local linear approximations). Indeed, trends are the most intuitive feature of a time series: One easily recognizes its upward and downward episodes and it seems natural to use them for series description and analysis. Such a description is intrinsically multiscale since each non-trivial process exhibits juxtaposition of trends of different duration and steepness depending on the observational scale.

The proposed analysis is based on piecewise linear approximations of the analyzed time series. Such approximations unavoidably depend on the characteristic time scale of the analysis and involve a tradeoff between quality and detail. We formulate (see Section 2.3) an optimality criterion for a local piecewise linear approximation and use it in a multiscale fashion to detect trends in a time series at *all* possible scales. Global piecewise linear approximations can then be constructed from such local trends. A hierarchy formed by the local trends is used for quantitative analysis.

The problem of piecewise interpolation of time series has been given significant attention in the context of image processing (see for example [1, 2, 3]). The focus was on constructing an optimal piecewise linear approximation $L_\epsilon(t)$ with minimal number of segments for given error ϵ (deviation from the original signal). On the contrary, we concentrate on finding a whole hierarchy of consecutively more detailed approximations.

MTA is data adaptive: it creates a natural partition of the observational time interval uniquely linked to the trend structure of the analyzed series. This contrasts with more conventional methods of self-affine analysis, which commonly use dyadic, ternary, etc. partition schemes independent of the series analyzed. On one hand, our analysis is deterministic: we work with a single observed realization and look for its unique properties. On the other hand, the overall statistics resulting from MTA allow one to make decisive conclusions about the process in general.

Areas for application of MTA include:

- *Descriptive and exploratory data analysis.* Computationally effective trend decomposition naturally complements a standard data miner's toolbox. Conveniently, MTA does not rely on any assumptions about the analyzed time series (e.g. stationarity or existence of higher moments).
- *Self-affine analysis.* Particularly, MTA provides a way to extract local fractal properties of the processes.
- *Hierarchical analysis.* The key element of MTA is construction of a hierarchical tree T_X that represents the multiscale trend structure of the analyzed time series $X(t)$. As a result MTA allows one to analyze time series with methods borrowed from the theory of hierarchical scaling complexities [8]. Particularly, Horton-Strahler indexing provides a natural way to consider scaling laws for trends.
- *Correlation analysis.* MTA allows one to detect non-linear correlations, particularly those caused by the presence of amplitude modulation and non-linear long-term trends.

The paper is organized as follows: Section 2 introduces the basic notions and describes the computational algorithm for Multiscale Trend Decomposition (MTD). Methods of MTD-based self-affine analysis comprise Section 3. Section 4 introduces hierarchical analysis of time series. Correlation analysis is described in Section 5. Fractional Brownian walks and Mandelbrot cascade measures are used to illustrate methods of Section 3 - 5. Section 6 concludes.

2 Multiscale Trend Decomposition (MTD)

The core of the MTA is construction of a hierarchical tree T_X that describes the trend structure of a given time series $X(t)$. Trend is defined here as a linear least square approximation of $X(t)$ at a subinterval of the observational time interval. The tree T_X is formed step-by-step, from the largest to the smallest scales: First, we determine the longer trends, then look for the shorter and shorter trends against the background of already established ones, all the way down the hierarchy of scales. The larger the scale at which the trend is observed, the higher the level of the corresponding vertex within the tree. The root (top vertex) of the resulting tree T_X corresponds to the global linear trend of $X(t)$; each internal vertex corresponds to a distinct local trend, the leaves (vertices with no descendants) to the elementary linear segments of the original time series $X(t)$: $[X(t_i), X(t_{i+1})]$. The union of leaves thus coincides with $X(t)$.

A recursive procedure for constructing the tree T_X is described below.

2.1 Scheme of the decomposition

Without loss of generality we presume that the time series $X(t)$ is observed at a finite number of epochs within the time interval $[0, 1]$. At the first step of MTD the whole

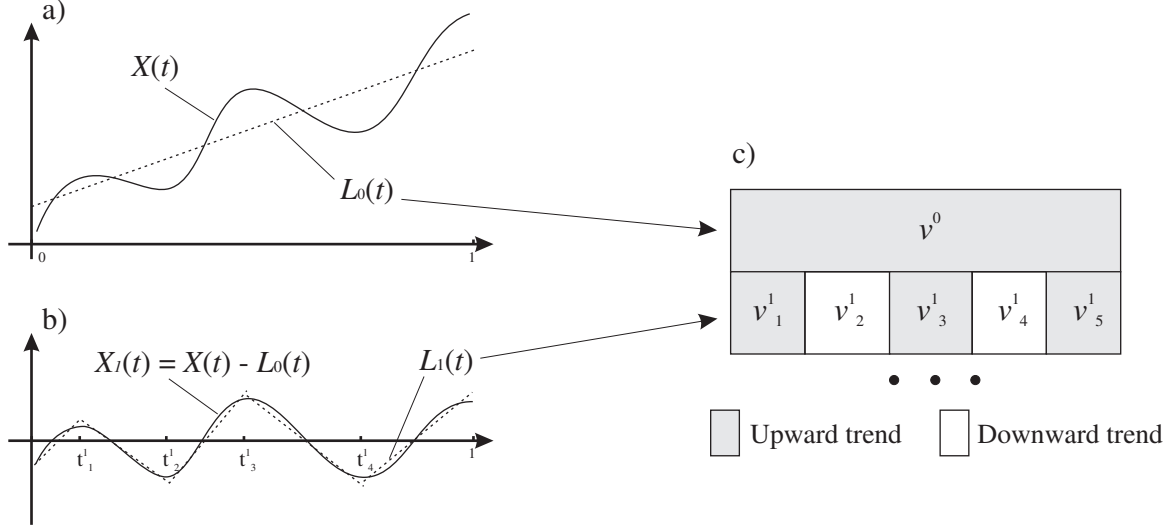


Figure 1: Scheme of the Multiscale Trend Decomposition (MTD). a) At zero step $X(t)$ is approximated by its global linear trend $L_0(t)$. b) Detrended series $X_1(t) = X(t) - L_0(t)$ is approximated by the piecewise linear function $L_1(t)$, the whole analysis is then repeated at each of subintervals $[t_i^1, t_{i+1}^1]$. c) Resulting hierarchy of trends. See Section 2 for details.

time series $X(t)$, $t \in [0, 1]$ is approximated by a single trend — the linear least square fit $L_0(t)$ (Fig. 1a).

This trend forms the vertex v^0 at the level 0 (the root) of the resulting hierarchical tree T_X (Fig. 1c). It is also convenient to say that the root of T_X corresponds to the whole time interval $[0, 1]$, and vice versa. At the next step we determine secondary trends on the background of the first global one. For this we consider the deviation $X_1(t) = X(t) - L_0(t)$, $t \in [0, 1]$ of $X(t)$ from its linear trend $L_0(t)$ and approximate it by a piecewise linear (discontinuous) function $L_1(t)$ (Fig. 1b). The most delicate part of the analysis — choosing the optimal number n^0 of segments for this approximation — is described below in Section 2.2. The approximation $L_1(t)$ results in partition of the time interval $[0, 1] = I^0$ into n^0 nonoverlapping subintervals $I_i^1 = [t_i^1, t_{i+1}^1]$, $i = 1, \dots, n^0$, with $t_1^1 = 0$, $t_{n^0+1}^1 = 1$. The linear segments $l_i^1(t)$ that comprise $L_1(t)$ are determined by the least square fit of $X(t)$ within corresponding subintervals. They form n^0 vertices v_i^1 , $i = 1, \dots, n^0$ at level 1 of the tree T_X . The enclosures $I_i^1 \subset I^0$ are reflected in the structure of the tree T_X by the fact that the vertices corresponding to subintervals I_i^1 are descendants of the root, which corresponds to I^0 .

Repeating the above procedure at arbitrary interval I_i^1 from level 1 we form n_i^1 ternary linear trends, each determined by the least square fit of $X(t)$ at a subinterval $I_j^2 \subset I_i^1$, $j = 1, \dots, n_i^1$. The union of $N_2 = \sum_{i=1}^{n^0} n_i^1$ such trends descending from all the trends of level 1 form level 2 of the tree T_X . To index the vertices (local trends) at level 2 we use the natural ordering induced by the corresponding time partition: v_i^2 (l_i^2) denotes the

vertex (trend) that corresponds to the time subinterval $I_i^2 = [t_i^2, t_{i+1}^2]$, $i = 1, \dots, N_2$.

Repeating the same procedure at each time interval of level l , $l \geq 0$ we form level $(l + 1)$. It consists of

$$N_l = \sum_{i=1}^{N_{l-1}} n_i^{l-1}$$

subintervals (vertices). By construction, $N_0 = 1$ and $N_k < N_p$ for $k < p$. We depth of the resulting tree is denoted by L .

Each level l of the tree T_X corresponds to a piecewise linear approximation $L_l(t)$ of the time series $X(t)$ as well as to the induced partition $I^l = \{I_i^l, i = 1, \dots, N_l\}$ of the observational interval I^0 . The global piecewise linear approximation $L_l(t)$ at level l is a union of local linear approximations $l_i^l(t)$, $t \in I_i^l = [t_i^l, t_{i+1}^l]$, $i = 1, \dots, N_l$, and $I^0 = \cup_{i=1}^{N_l} I_i^l \forall l$.

By r_i^l we denote the length of subinterval I_i^l , and by e_i^l the rms deviation of $X(t)$ from its linear fit $l_i^l(t)$ at this subinterval:

$$e_i^l = \sqrt{\sum_{t \in I_i^l} (X(t) - l_i^l(t))^2}. \quad (1)$$

The total fitting error E_l at the level l is given by

$$E_l^2 = \sum_{i=1}^{N_l} (e_i^l)^2 = \sum_{t \in I^0} (X(t) - L_l(t))^2. \quad (2)$$

All vertices (subintervals) at a given level of T_X result from the same number of divisions of the initial interval $[0, 1]$. However, in many applications it is desirable to work with approximations characterized by a similar scale of observed trends, independently of the division history. To take this into account we consider the modified tree M_X obtained from T_X by the following procedure. The first two levels of M_X are the same as that of T_X . Each consecutive level is formed by division of only one of the existing subtrends and leaving all the other unchanged. A subtrend v_i^l to be divided corresponds to the maximal improvement of the fitting quality $\Delta = (e_i^l)^2 - \sum (e_c^{l+1})^2$, where c runs over the indexes of children of the vertex i . We will call T_X the topological and M_X the metric tree associated with the series $X(t)$. To avoid excessive notations we will use the same indexing for both the trees T_X and M_X stating each time which one is considered.

2.2 Optimal piecewise linear approximation

Here we describe a procedure for finding the optimal piecewise linear approximation $L(t)$ of a series $X(t)$ at a given time interval. Without loss of generality we suppose that the interval is $[0, 1]$. The problem, of course, is in finding the optimal tradeoff between the number N of linear segments within $L(t)$ and the corresponding fitting quality E .

Clearly, the larger the number N , the better the resulting fit. Our goal is to depict by linear segments only the most prominent large-scale trends of $X(t)$ leaving the smaller fluctuations for the later steps of the decomposition. To solve this problem we employ the function

$$H(N, E) = -\frac{\log(E/E_0)}{N-1}, \quad (3)$$

where E_0 is the fitting error of the global linear approximation $L_0(t)$ of $X(t)$ on $[0, 1]$. This function measures the quality of a piecewise linear approximation $L(t; N, E)$ which consists of N linear segments and has total fitting error E . The optimal approximation $L(t; N^*, E^*)$ corresponds to the maximum of $H(N, E)$:

$$H(N^*, E^*) = \max_{N, E} H(N, E). \quad (4)$$

Geometrically, consider the plane $(N, \log(E/E_0))$, N being the number of linear segments within a piecewise linear approximation of $X(t)$ on $[0, 1]$, and E the total fitting error. The global linear approximation $L_0(t)$ at the whole interval $[0, 1]$ corresponds to the point $p_0 = (1, 0)$. An arbitrary piecewise approximation $L_i(t)$ corresponds to the point $p_i = (N_i, \log(E_i/E_0))$, $N_i \geq 1$, $E_i \leq E_0$. The slope of the linear segment $[p_0, p_i]$ shows the increase of the fitting quality per one additional segment of approximation. By the criterion (3,4) we chose the approximation with the maximal quality increase.

With the above criterion (3,4) one can find the optimal approximation by a full search over all possible partitions of $[0, 1]$ by epochs of $X(t)$ into $N = 2, 3, \dots$ subintervals. However, the computational complexity of such an approach depends exponentially on the number of observations so it can hardly be used in practice. In Section 2.3 below we introduce an optimized search based on the idea that partition epochs should correspond to the prominent edges of the analyzed series $X(t)$.

2.3 Optimized search

The idea of the optimized search is to reasonably reduce the set of possible partition epochs by considering only those at which $X(t)$ significantly changes its slope — edge points.

The edge points are determined by the following recursive procedure illustrated in Fig. 2.

At the first step we choose the epochs (t_1, t_2) corresponding to the maximum and minimum of the detrended function $X_1(t) = X(t) - L_0(t)$, where $L_0(t)$ is a least-square linear fit of $X(t)$ in $[0, 1]$. If one of these epochs coincides with the interval boundary (say, $t_1 = 0$) only the remaining epoch (t_2) is considered. If both these epochs coincide with the interval boundaries, we redefine $L_0(t)$ as the line connecting $X(0)$ and $X(1)$ and repeat the procedure. As a result we have one or two partition epochs within the initial interval; they divide it into two or three subintervals respectively. The procedure is now repeated for each of these subintervals, producing two to six new partition epochs. Together with already selected ones, they divide the initial interval into, respectively,

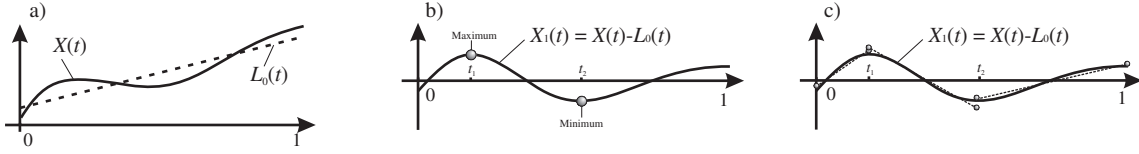


Figure 2: Scheme of detection of edge points. a) At zero step $X(t)$ is approximated by its global linear trend $L_0(t)$. b) Epochs (t_1, t_2) of global maximum and minimum of the detrended series $X_1(t) = X(t) - L_0(t)$ are located. c) Analysis is repeated at each of subintervals $[0, t_1]$, $[t_1, t_2]$, and $[t_2, 1]$.

four to nine subintervals, etc. The partition stops when the predefined number $(N_h - 1)$ of partition epochs is collected; this corresponds to N_h subintervals.

With $(N_h - 1)$ possible partition epochs there are $(2^{N_h-1} - 1)$ ways to divide the interval into $2, \dots, N_h$ subintervals. The optimal — according to (3,4) — partition can be found by $(2^{N_h-1} - 2)$ operations.

To further reduce the computation volume, we first choose the optimal one from $(N_h - 1)$ partitions formed by $(N_h - 2)$ partition epochs. Next, only the $(N_h - 2)$ epochs that form this partition are used to find the optimal partition with $(N_h - 3)$ partition epochs, etc. Finally, we use criterion (3,4) to choose the optimal from $(N_h - 1)$ partitions, each having a distinct number of subintervals ranging from 2 to N_h . This way we reduce the number of operations to $(N_h^2 - N_h - 2)/2$.

Clearly, the above optimization may produce a piecewise function which does not coincide with the optimal one resulting from applying the criterion (3,4) to the whole variety of possible partitions. As such, this optimization should be considered as a computationally effective approximation of the result. Extensive numerical experiments show that it is reasonably good for a wide range of time series including fractional Brownian motions with different Hausdorff measures and self-affine processes coming from geophysical observations.

2.4 Examples

In this section we show examples of MTD and illustrate different ways to visualize the results of the decomposition.

Fig. 3 shows four levels, $l = 0, 1, 2$, and 10 of MTD for a fractional Brownian walk with Hausdorff dimension $Ha = 0.7$. Panel a) shows the analysed series $X(t)$ and the piecewise linear approximations $L_l(t)$, $l = 0, 1, 2, 10$ from the MTD, while panel b) shows the four corresponding levels of the tree M_X .

One can see how the fitting quality improves with the number of linear segments: each consecutive approximation tries to account for the most prominent variations of $X(t)$ adding the least possible number of new segments. For example, starting with the three segments of the decomposition $L_1(t)$ at level 1, it is clearly more efficient to improve the leftmost segment, which exhibits large deviations around $t = 0.1$, than work with the

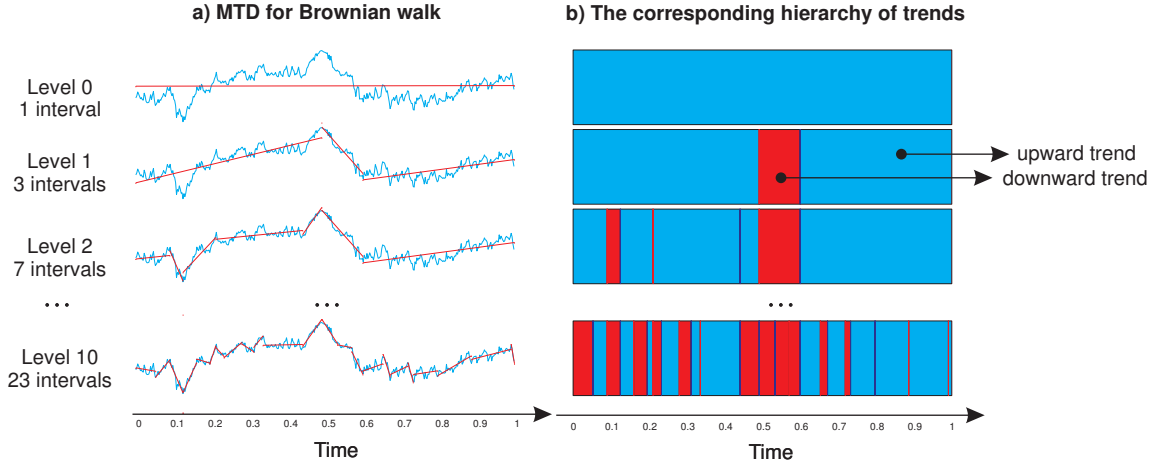


Figure 3: Example of MTD for a Fractional Brownian walk with Hausdorff measure $Ha = 0.7$. a) Piecewise linear approximations at levels $l = 0, 1, 2, 10$. b) Corresponding hierarchical tree.

central or rightmost one. When work is done with the largest deviation (see level 2) we proceed to the smaller ones.

The function shown in Fig. 4a on the background of its tree M_X is a sum of three sinusoids with different frequencies.

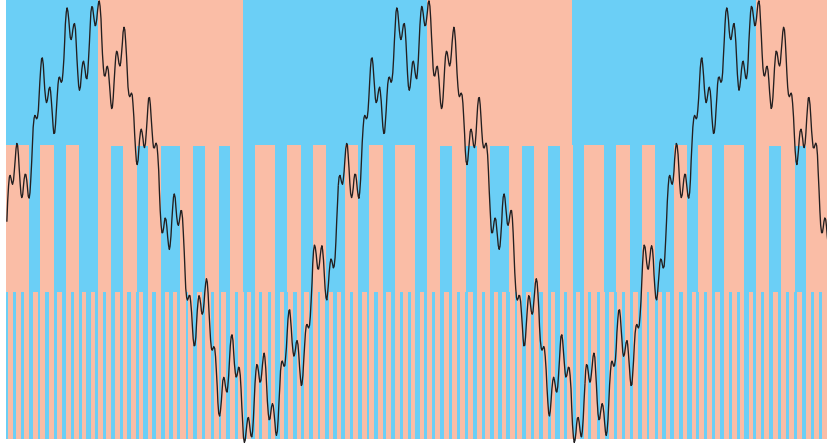
The amplitudes are chosen in such a way that the largest fluctuations are carried at the smallest frequency, intermediate at the second largest, and smallest at the highest one. This structure is clearly depicted by the decomposition with each separate level responsible for a distinct frequency (see panels b), c), and d)).

Two more examples are given in Fig. 5 where we show only the signals $X(t)$ and the upper levels of their trees M_X , which is enough to understand the shape of corresponding piecewise linear approximations. Decomposition for the famous Devil's Staircase is shown in Fig. 5a: it gives the exact description of the staircase structure. Figure 5b shows a decomposition for modulated oscillations with time-dependent frequency. Contrary to the panel a) here we use color-code to depict slope changes (from downward to upward or vice versa), not their directions. In this example one can see how the amplitude of oscillation is reflected in the decomposition: the higher the amplitude, the higher the level at which it is first detected.

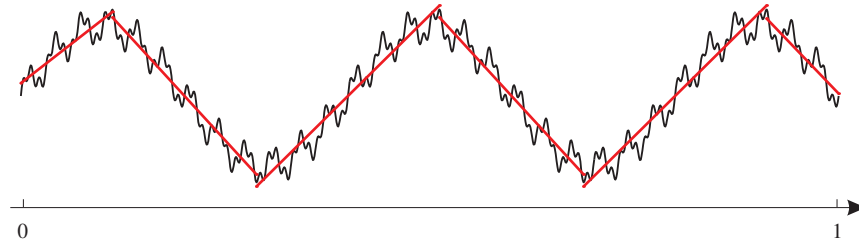
2.5 On the numerical parameter N_h

The only numerical parameter of our algorithm is the maximal number N_h of secondary trends (see Section 2.3). Large values of N_h contribute to the computational complexity, while small values may prevent fast detection of optimal approximation and create superfluous levels of the hierarchy T_X . Numerous experiments suggest the value $N_h = 5$ as the optimal tradeoff, and we use it for all experiments presented in this paper.

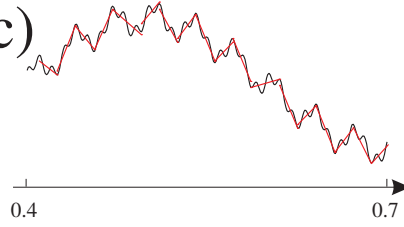
a)



b)



c)



d)

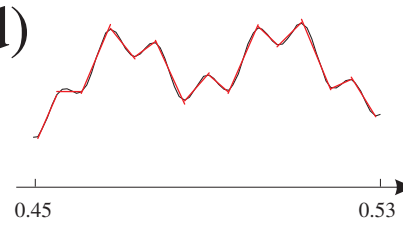


Figure 4: Example of MTD for the sum of three sinusoids, $X(t) = \sin(5\pi t) + \frac{1}{5}\sin(60\pi t) + \frac{1}{10}\sin(200\pi t)$. a) $X(t)$ on the background of three levels from its MTD decomposition. b) Piecewise linear approximation corresponding to the top level of MTD shown in panel a). c) Fragment corresponding to the middle level of a). d) Fragment corresponding to the bottom level of a).

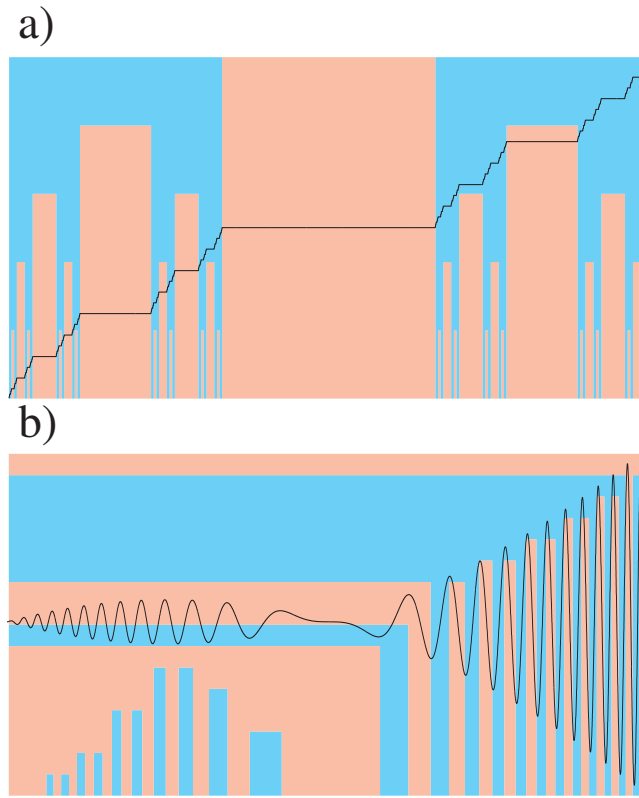


Figure 5: Examples of MTD. a) Devil's Staircase (5 upper levels of MTD are shown). b) Modulated sinusoid with time-dependent frequency (15 levels are shown).

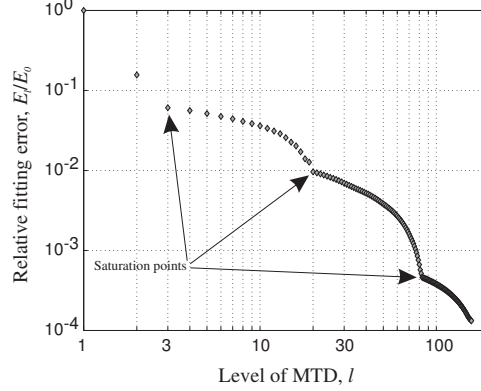


Figure 6: Illustration of a procedure for removing unnecessary levels of MTD (for the signal shown in Fig. 4). Prominent saturation points correspond to the three levels shown in Fig. 4

Clearly, with $N_h = 5$ we are not insured from creating unnecessary levels. For example the division of Fig. 4b consists of 6 ($> N_h = 5$) linear segments, so it could not be obtained by a single division of the original series. In fact this is level 2 of the original hierarchy M_X . Analogously, the intermediate division of Fig. 4a (see also Fig. 4c) corresponds to level 19, and the bottom one (Fig. 4d) to level 82.

The simple procedure used to remove unnecessary levels is illustrated in Fig. 6 where we show the fitting error E_l/E_0 for all levels l of the tree M_X constructed for the signal of Fig. 4a. The prominent edge points show the three levels at which saturation of the fitting quality is reached; only these three levels are left in Fig. 4a.

If the analyzed tree has only less-than-5-fold partitions (which is the case for the Devil's Staircase of Fig. 5a) the above procedure is unnecessary. The properties of this procedure and conditions for its use are beyond the scope of the present paper.

3 Self-affine properties of MTD

In this section we demonstrate how self-affine properties of a time series are reflected in its decomposition M_X .

Recall [4] that statistical properties of a self-affine time series $X(t)$ remain the same under the transformation

$$\begin{cases} t' &= rt, \\ X' &= r^{Ha} X. \end{cases} \quad (5)$$

That is, when one changes the observational time scale by a factor of r , the scale of measurements should be changed by a factor of r^{Ha} in order to preserve the characteristic statistical features of $X(t)$. The parameter Ha is called Hausdorff measure; it is related to the fractal dimension D of a self-affine time series as $Ha = 2 - D$ [4]. Accordingly, for one-dimensional time series the Hausdorff measure may take values within the range $0 <$

$Ha < 1$. A useful interpretation of Ha comes from the character of correlations between the time series increments: $\Delta_i = X(t_i) - X(t_{i-1})$. Negative correlations between Δ_i and Δ_{i+1} lead to high fluctuations of $X(t)$ and as a result to absence of pronounced trends; this situation corresponds to small values of Hausdorff measure: $Ha < 1/2$. Positive correlations — leading to existence of long-term trends — correspond to $Ha > 1/2$. For a process with independent increments (e.g. Brownian walk) one has $Ha = 1/2$.

To estimate the Hausdorff measure of observed time series one typically considers the dependence of a convenient measure of its variation on the length of a corresponding observational interval [4]. In our case the appropriate variation measure can be chosen as the fitting error E_l (2) of M_X at level l . According to (5), for a self-affine series $X(t)$ we expect to observe a power-law relation

$$\frac{E_l}{E_0} = N_l^{-Ha} = R_l^{Ha}, \quad (6)$$

where N_l is the number of segments at the level l , $R_l = N_l^{-1}$ is their mean length.

As a model example we consider fractional Brownian walks (FBWs) with Hausdorff measures in the range $0 < Ha < 1$.

Figure 7a shows trajectories and the corresponding (N_l, E_l) -scalings for three FBWs with $Ha = 0.1, 0.5$, and 0.9 . Figure 7b shows the value $b(Ha)$ estimated by the best linear square fit from the relation

$$\log(E_l/E_0) = -b \log(N_l) \quad (7)$$

based on MTD of 2100 independent FBWs; to remove statistical fluctuations we averaged b over 100 FBWs for each value of Ha . As seen in Fig. 7b, the scaling (6) clearly holds for $Ha > 0.3$; the deviations observed at the smaller values of Ha are due to the fact that the corresponding FBWs become noisier and hardly display pronounced trends. This effect is typical for self-affine analysis (e.g., see [5]). To neglect it we consider the integrated signal $Y(t) = \sum_{s \leq t} X(s)$. Estimations of the slope $b(Ha)$ for integrated FBWs are presented in Fig. 7c. The linear relation $b(Ha) = Ha + 1$ is now observed for $0 < Ha < 0.6$, the change of slope compared to Fig. 7b is due to the integration procedure.

Another way to estimate Ha is to consider the error-length dependence for all individual linear segments comprising M_X :

$$\frac{e_i^l}{E_0} = (r_i^l)^{Ha+1/2}, \quad l = 1, \dots, L, \quad i = 1, \dots, N_l. \quad (8)$$

The difference in the power exponents of relations (6) and (8) is explained by the fact that the former deals with averaged statistics, while the latter deals with characteristics of individual intervals. Figure 8 illustrates the error-length dependence (8) for FBWs with $Ha = 0.1$ and $Ha = 0.9$.

Importantly, MTD provides a convenient basis for estimation of local Hausdorff measures $Ha(t)$. Consider all the intervals from T_X that cover epoch t . At each level l of

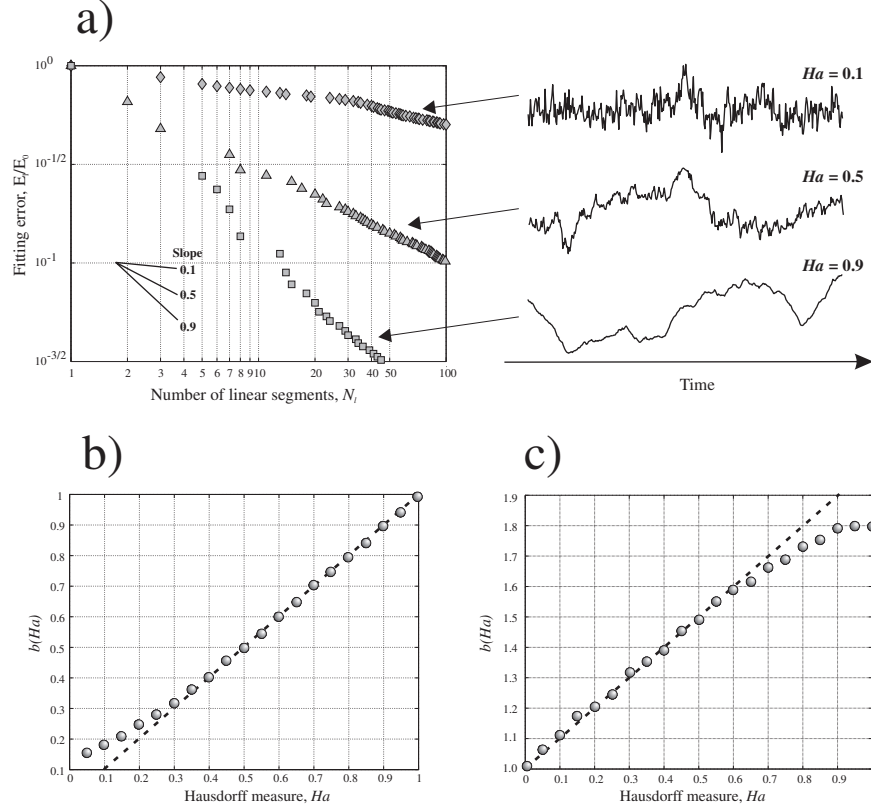


Figure 7: Relation between Hausdorff measure and error scaling of MTD levels for fractional Brownian walks (FBW). a) Trajectories of FBWs with $Ha = 0.1, 0.5, 0.9$ and corresponding error scalings. b) Relation $b(Ha)$ for FBWs, $0 \leq Ha \leq 1$, values of b averaged over 100 realizations of FBW for each value of Ha . c) The same as b) for integrated FBWs.

Figure 8:

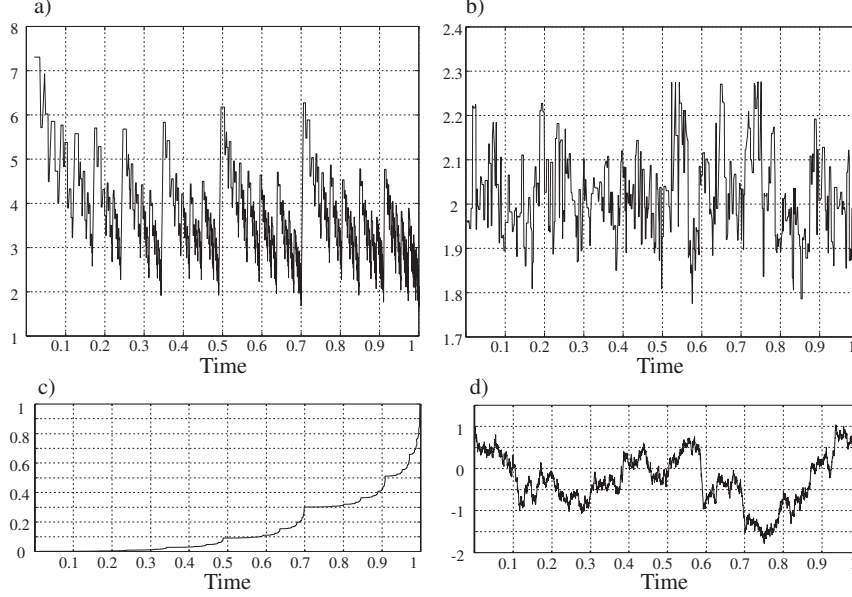


Figure 9: Estimation of local Hausdorff measures, $Ha(t)$ for a multifractal (Mandelbrot cascade measure) (panel a) and monofractal (Brownian walk) (panel b). Corresponding time series are shown in panels c) (multifractal) and d) (monofractal).

T_X there is one and only one such interval; we use the index ${}^l_{(t)}$ to denote this interval and all its characteristics. The local Hausdorff measure $Ha(t)$ is estimated now from the relation

$$\frac{e^l_{(t)}}{E_0} = \left(r^l_{(t)}\right)^{Ha(t)+1/2}, \quad l = 1, \dots, L. \quad (9)$$

Figures 9a,b show the dynamics of the local Hausdorff measure for multi- and monofractals. We use a Mandelbrot cascade measure $M(0.7, 0.3; 0.3, 0.7)$ as a model example of a multifractal (Fig. 9c), and a Brownian walk as that of a monofractal (Fig. 9d). The definition of Mandelbrot cascade measure is given in Appendix A. Note that the range of $Ha(t)$ variation for the monofractal (Fig. 9b) is an order of magnitude less than that for the multifractal (Fig. 9a).

The points $(e^l_{(t)}, r^l_{(t)})$ used in (9) to estimate the local Hausdorff measure are extracted from the whole set (e^l_i, r^l_i) of (8). This suggests a method for detecting multifractality in $X(t)$: the larger the scattering of the points (e^l_i, r^l_i) , the larger the probability that the observed series is a multifractal. Formal statistical tests can be easily constructed from this general principle based on the particular problem at hand. The character of temporal variations of $Ha(t)$ (Figs. 9a,b) can be also used in such tests. An example of the scattering (e^l_i, r^l_i) is shown in Fig. 10 for mono- and multifractals of Fig. 9. In this model example the difference is obvious.

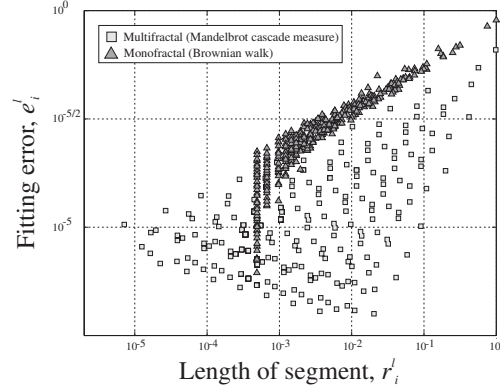


Figure 10: Error-length dependence for multi- and monofractals of Fig. 9. Note that the point scattering is significantly larger for the multifractal.

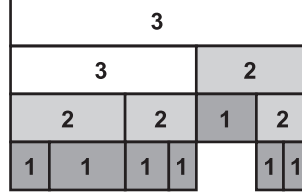


Figure 11: Horton-Strahler indexing.

4 Hierarchical scaling

The appropriate ordering of vertices within a tree T_X is very important for meaningful description and analysis of the series $X(t)$. The problem of such an ordering becomes not trivial as soon as the tree is not uniform (i.e. is not formed by applying the same deterministic division rule to each of its vertices). A befitting way to solve this problem is given by the Horton-Strahler topological classification of ramified patterns [6, 7, 8] illustrated in Fig. 11: One assigns orders to the vertices of the tree, starting from $k = 1$ at leaves (vertices with no descendants).

The order of an internal vertex equals the maximal order m of its descendants, if they are distinct, and $m + 1$ if they are all equal. Originally introduced in geomorphology by Horton [6] and later refined by Strahler [7], this classification is shown to be inherent in various geophysical, biological, and computational applications [8, 9, 10, 11].

As a result of the Horton-Strahler indexing of the tree T_X , each of its vertices is characterized by an order k , length r of the corresponding partition interval, and the error e of the linear least square fit of $X(t)$ on this interval. The scaling behavior of $X(t)$ can be described by the exponents of the relations:

$$N(k) \sim 10^{-B_N k}; \quad R(k) \sim 10^{B_R k}; \quad E(k) \sim 10^{B_E k}. \quad (10)$$

Here $N(k)$ is the number of vertices of order k , $R(k)$ and $E(k)$ are the values of r and e

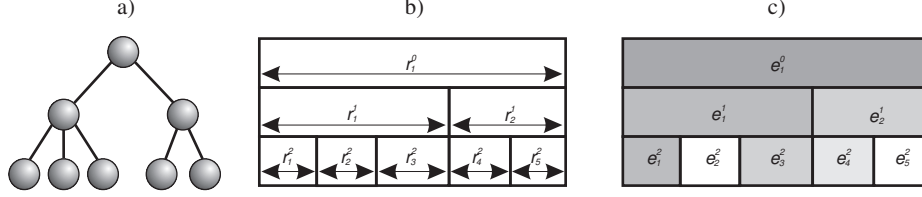


Figure 12: Three levels of detail in the description of a time series in terms of its MTD decomposition. a) Topological. b) r -metric, based on the interval partition. c) e -metric, based on local linear fit of the series. See details in Section 4.

averaged over the vertices of order k .

The relation between the number $N(k)$ of vertices of order k and their average length $R(k)$ determines the fractal dimension d of the tree T_X [9]:

$$N(k) = R(k)^{-d}. \quad (11)$$

Combining (10) and (11) we find:

$$d = \frac{B_N}{B_R}. \quad (12)$$

The structure of the tree T_X can be considered at different levels of detail: First, one can consider only the topological structure (Fig. 12a), where the position of each vertex is uniquely determined by its parent (the nearest vertex placed closer to the root); and any permutation of siblings (the vertices with the same parent) does not change the tree. Each vertex is characterized by its Horton-Strahler index, and the only constraint on a tree resulting from MTD is the maximal possible number N_h of siblings, that is subtrends within a given trend. Next, one can add the information on interval partition (Fig. 12b): The siblings become ordered according to the partition of the interval corresponding to their parent. Each vertex v_i is additionally characterized by the length r_i and the following conservation law holds:

$$r_i = \sum r_c, \quad (13)$$

where c runs over the indexes of the children of the element i .

Finally, (Fig. 12c) one considers error characteristics e_i , which describe the quality of the linear fit of $X(t)$ within the corresponding time interval. In terms of these errors the system becomes dissipative:

$$e_i \geq \sum e_c, \quad (14)$$

with the same meaning of subindexes as in (13).

The exponents $B_{N,R,E}$ of (10) reflect different statistical properties of the tree T_X : B_N describes its topological structure while B_R and B_E relate to the metric structures based, respectively, on properties of interval partition (r -metric) and piecewise linear fit (e -metric).

For illustration we again use FBWs with different Hausdorff measures.

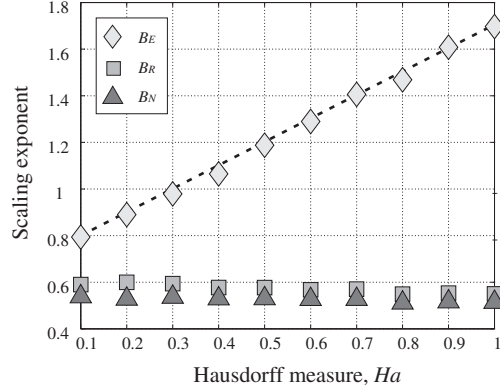


Figure 13: Dependence of scaling exponents $B_{E,R,N}$ (Eq. (10)) on the Hausdorff measure Ha of FBWs. Dashed line is $B = 0.7 + Ha$.

Figure 13 shows the dependence of the exponents $B_{N,L,E}$ on the Hausdorff measure $0 \leq Ha \leq 1$. The estimations are averaged over 100 FBWs for each value of Ha . The exponents B_N and B_R are nearly constant: $B_N \approx 0.52$, $B_R \approx 0.57$, while for the exponent B_E we observe the linear dependence:

$$B_E = 0.7 + Ha \approx \log_{10}(5) + Ha. \quad (15)$$

These results have an important interpretation: All FBWs with Hausdorff measure in the range $0 \leq Ha \leq 1$ have the same topological and r -metric structures in terms of MTD tree T_X . Particularly, trees T_X corresponding to different Ha have the same fractal dimension $d = B_N/B_R \approx 0.9$. The only characteristic that depends on the Hausdorff measure is the fitting error (e -metric), that is the degree of variation of $X(t)$ within a given interval.

5 Correlation analysis

One of the important applications of MTA is correlation analysis of time series. The major drawback of classical correlation analysis is that interpretation of its results may be completely ruined by the presence of long-term trends and/or modest amplitude modulations of signals. The MTA can naturally avoid these problems by depicting the essential local properties of the analyzed series.

We start this section by introducing two MTD-based measures of similarity for time series. One is based solely on the time interval partition induced by M_X ; another takes into account the directions (upward vs. downward) of local trends.

5.1 Distance between partitions

Each level l of the tree M_X (Section 2) corresponds to a partition of the time interval $[0, 1]$ into N_l nonoverlapping subintervals. Since each of these subintervals corresponds

to a distinct observed trend of the series $X(t)$, the problem of comparison of two such partitions naturally arises. Below we introduce the distance between two partitions.

Consider the space Ω of finite partitions of the unit interval $[0, 1]$. Each partition A is defined by a finite number n_A of points; the boundaries 0 and 1 are included in all partitions:

$$A = \{0 = a_0 < a_1 < \dots < a_{n_A} < a_{n_A+1} = 1\}.$$

The trivial partition U consists only of boundary points: $U = \{0, 1\}$.

For $A, B \in \Omega$ we say that B is a subpartition of A ($B \subset A$) if all points from A are among points from B ; this imposes a partial order on Ω . A union $A \cup B$ is defined as the partition consisting of the points included in either A or B , without repetitions. An intersection $A \cap B$ is defined as the partition consisting of points included in both A and B .

An asymmetric distance $m(A, B)$ from A to B ($A, B \in \Omega$) can be defined as

$$m(A, B) = \sum_{i=1}^{n_A} \min_{0 \leq j \leq n_B+1} \{|a_i - b_j|\}, \quad (16)$$

which gives for the trivial partition

$$m(A, U) \equiv m(A) = \sum_{i=1}^{n_A} \min\{a_i, 1 - a_i\}$$

The distance (16) is interpreted as the minimal correction to A that makes B its subpartition: $B \subset A'$, where A' stands for the corrected version of A .

The following properties of $m(A, B)$ follow directly from the definition (16):

1. $0 \leq m(A, B) < \infty$;
2. $m(A, B) = 0$ iff $B \subset A$;
3. Additivity with respect to A : $m(A_1 \cup A_2, B) = m(A_1, B) + m(A_2, B)$;
4. Monotonicity with respect to B (the triangle inequality): $m(A, B_1 \cup B_2) \leq m(A, B_1) + m(A, B_2)$.

It is convenient to consider the symmetric function

$$\mu(A, B) = \max\{m(A, B), m(B, A)\}, \quad (17)$$

whose small values signal that the partitions A and B are similar. Note that μ is not a distance since it does not satisfy the triangle inequality. The reciprocal μ^{-1} may serve as a measure of partition correlation.

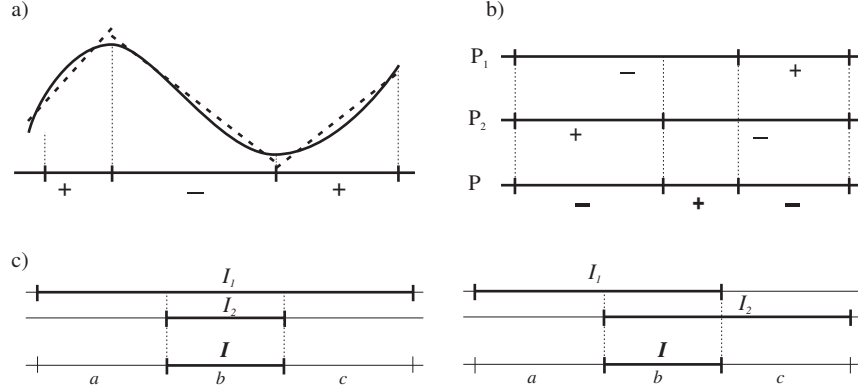


Figure 14: Signed partition corresponding to a piecewise linear approximation (panel a), union of signed partitions (panel b), and triplet (a, b, c) for an interval of a union of partitions. see Section 5.2.

5.2 Slope sign correlation

Here we introduce the correlation function that describe similarity between two piecewise linear approximations $L^1(t)$ and $L^2(t)$ of $X(t)$, $t \in [0, 1]$. (We use upper indexes in order not to mix these arbitrary approximations with $L_1(t)$, and $L_2(t)$ at the first and second levels of the decomposition.) This correlation function is based on the coarse information about trends from $L^i(t)$: We take into account only their directions — upward vs. downward.

First, we introduce the signed partitions P_1 and P_2 of the interval $[0, 1]$. They are formed by the intervals of constant sign of the slope of $L^i(t)$, $i = 1, 2$ (see Fig. 14a).

A subinterval from P_i is assigned the sign "+" if the corresponding trend of $L^i(t)$ is upward, and "-" if it is downward. Second, we define the signed partition P as a union of P_i , $i = 1, 2$ with the signs determined by multiplication of the signs of the corresponding subintervals from P_i (Fig. 14b). As a result, the positive intervals of P correspond to matching (up to direction) trends of L^1 and L^2 , while negative to unmatched ones.

Each subinterval I of the partition P is formed by intersection of two subintervals $I_i \in P_i$, $i = 1, 2$; two general variants of such an intersection are shown in Fig. 14c. A subinterval I is assigned a triplet (a, b, c) defined as shown in Fig. 14c: b is the length of the intersection $I_1 \cap I_2$, while a and c are the lengths of those parts of I_i that are not included in the intersection. The triplet is normalized: $a + b + c = 1$. It describes how good is the matching of intervals I_i : the meaning of b is clear; the best matching for a given b corresponds to the case when the intervals' ends coincide, that is to $a \cdot c = 0$. The matching quality can be reflected in the weight

$$w = -\frac{(1-b) \log(1-b)}{a \log(a) + c \log(c)} = -\frac{(a+c) \log(a+c)}{a \log(a) + c \log(c)}, \quad (18)$$

lying within the range $0 \leq w \leq 1$.

The correlation function $r(L^1, L^2)$ is now defined as

$$r(L^1, L^2) = \sum_k r_k \cdot w_k. \quad (19)$$

Here the summation is taken over all the subintervals of the signed partition P ; r_k denotes the signed length of the k th subinterval, w_k is the corresponding weight (18).

The measure (19) is intentionally crude: it does not distinguish between steepness of the trends. More elaborate correlations can be easily defined following the scheme outlined above. Nevertheless, as we show in Section 5.3 below, even the roughest measure (16) is very effective in detecting non-linear correlations.

5.3 Examples

This section illustrates applications of MTD-based correlation analysis in the presence of long-term nonlinear trends and amplitude modulations.

5.3.1 Detection of correlation

Figure 15 displays the trajectories of two processes $F_i(t)$, $i = 1, 2$ coupled by the common underlying phenomenon which — by and large — makes them change their intermediate-scale trends synchronically. The most striking similarity between $F_i(t)$ is observed at the intervals $[0, 0.1]$ and $[0.2, 0.55]$. Also we note the synchronous peaks around $t = 0.675, 0.775, 0.975$ (more pronounced for $F_1(t)$.) At the same time, the coupling phenomenon is not a primary one in shaping the dynamics of $F_i(t)$, so their overall outlooks are still quite dissimilar. In such situations one is interested in detection and proper quantification of the observed non-linear coupling. The problem of such a quantification constitutes an important part of modern analysis of time series.

MTA suggests an effective way of solving this problem by comparing the trend structures of observed series at different scales. We decompose the observations $F_i(t)$ into trees M_i and calculate the distance μ (17) between different levels of these decompositions. The reciprocal μ^{-1} of the distance between the signals $F_i(t)$ is plotted as the function of the decomposition levels l_i , $i = 1, 2$ in Fig. 16a.

The diagonal ridge indicates pairs of levels with similar trend structures. The prominent upwell observed at the medium scales — $15 \leq l_1 \leq 18$, $14 \leq l_2 \leq 17$ — signals that this range is responsible for the observed coupling. The maximum $\mu^{-1} = 4.6$ corresponds to the levels $l_1 = 15$, $l_2 = 14$; we will refer to them as levels of maximal correlation (LMC). The piecewise linear approximations of $F_i(t)$ corresponding to the LMC are shown in Fig. 17. They clearly accentuate the observed coupling.

A typical shape of μ^{-1} for uncoupled time series is shown for comparison in Fig. 16b. The diagonal ridge is still observed, though it is more blurred. Existence of such a ridge is explained by the fact that partitions with a similar number of segments, even non-matching ones, are closer to each other in the sense of (17) than partitions with significantly different number of segments. Comparing Figs. 16a and b we conclude that

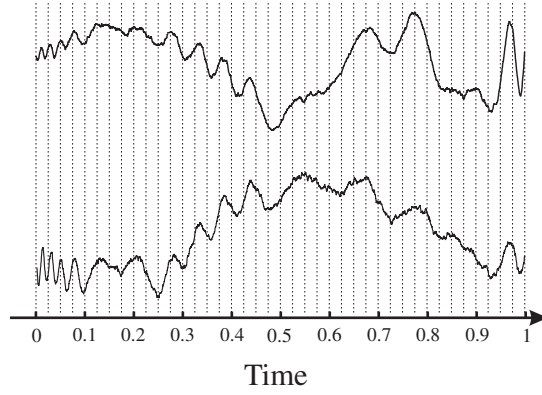


Figure 15: Two signals coupled by an unobserved phenomenon. The signals tend to change their intermediate trends synchronously, while their overall shapes are different. The striking similarity is observed at intervals $[0, 0.1]$ and $[0.2, 0.55]$. Note also the common peaks at $t = 0.675, 0.775, 0.975$. See details in Section 5.3.1.

Figure 16:

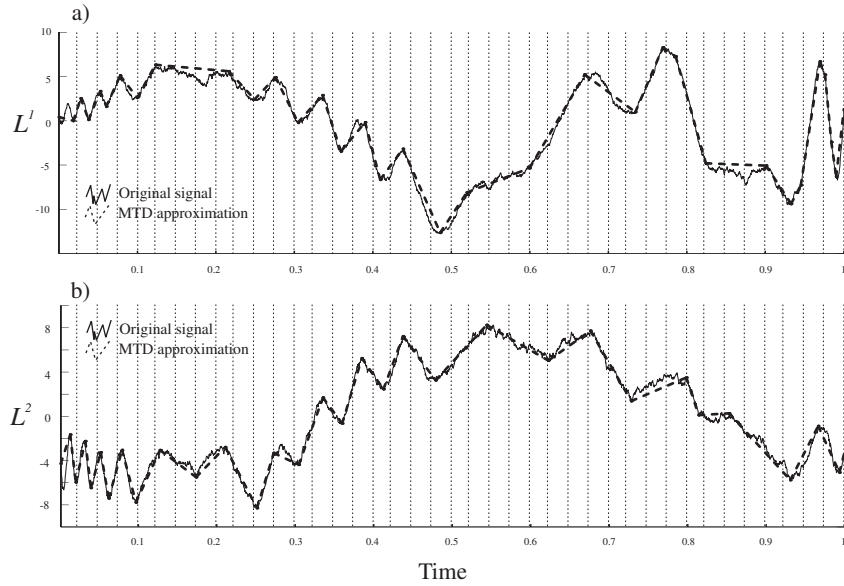


Figure 17: Piecewise linear approximations $L^i, i = 1, 2$ of the signals $F_i(t)$ from Fig. 15 at the levels of maximal correlation ($l_1 = 15, l_2 = 14$). These approximations depict the intermediate-scale variations responsible for the signals' coupling.

Figure 18:

the upwell observed in panel a is not a random one and is due to the correlation between the signals. A formal statistical test for establishing the significance of the observed peaks of μ can be easily constructed.

5.3.2 Quantification of detected correlation

As was shown in the previous section, MTA allows one to estimate non-linear correlations between signals; the value μ^{-1} may be considered as a measure of such correlation. Here we show how to evaluate the functional form of the coupling phenomenon responsible for the correlation detected.

To pose the problem formally, suppose that the observations $F_i(t)$, $i = 1, 2$ are formed by applying amplitude modulations $A_i(t)$ and adding non-linear trends $T_i(t)$ to the same base signal $X(t)$:

$$F_i(t) = A_i(t) \cdot X(t) + T_i(t) + \xi_i(t), \quad i = 1, 2. \quad (20)$$

Here $\xi_i(t)$ are measurement errors. In this model the correlation between signals $F_i(t)$ is due totally to the $X(t)$. The first problem is to reconstruct trends $T_i(t)$ and modulated signals $A_i(t) \cdot X(t)$ given the observations $F_i(t)$. Clearly, for reliable reconstruction one has to assume an appropriate rate of variation for the trends as well as a reasonably small noise-to-signal ratio. In practice, we assume that such conditions are satisfied if significant coupling has been detected by the correlation analysis of Section 5.3.1.

The idea of reconstruction is that the correlated parts $A_i \cdot X(t)$ should be described by the LMC of MTDs M_i (see Section 5.3.1). Accordingly, the trends $T_i(t)$ should be described by the higher-scale (less detailed) levels.

As a model example we again use the series of Fig. 15; in fact, they are produced by the model (20) with

$$\begin{aligned} X(t) &= \sin(400\pi t(t-0.5)(t-0.7)(t-1)); \\ T_1(t) &= 5 \sin(4\pi t^{3/2}); \\ T_2(t) &= -5 \cos(2\pi t^{3/2}); \\ A_1(t) &= \exp(2t); \\ A_2(t) &= 2 \exp(-t/3). \end{aligned} \quad (21)$$

The measurement errors $\xi_i(t)$ are modeled by independent Brownian walks so they also represent random drifts. The series $F_i(t)$ together with their components (21) are shown in Fig. 18.

The trends $T_i(t) + \xi_i(t)$ are estimated by the piecewise linear functions \hat{T}_i , formed by the parents of the vertices at the LMC, $l_1 = 15$, $l_2 = 14$. In other words, each of the linear segments at the levels l_i should be formed by a single non-trivial partition of one of the trends of \hat{T}_i . By single we mean that this is a one-time partition by

Figure 19:

the rules described in Section 2; by non-trivial — that each segment is divided into more than one subsegment. The modulated signals $A_i(t) \cdot X(t)$ are estimated then as $\hat{A}_i X_i(t) = (F_i(t) - \hat{T}_i(t))$, $i = 1, 2$.

The quality of these estimations is illustrated in Fig. 19 where we show real vs. estimated modulated signals $A_i X_i(t)$. The estimations are almost perfect at the intervals $[0, 0.1]$ and $[0.2, 0.55]$, (cf. Fig. 15 and its discussion in Section 5.3.1.) Generally, we catch well the oscillatory structure of the signals; that is their time-dependent frequencies and directions (upward vs. downward), while the amplitude estimation is less precise.

The estimations of Fig.19 can be further improved by means of various kernel smoothing techniques. The advantage of starting with MTD-based analysis is that its results can be used for optimization of the time-dependent kernel width.

With additional assumptions about the rate of variation for $A_i(t)$ one may pose the problem of reconstructing $X(t)$ given two, or more, modulated versions $A_i(t) \cdot X(t)$. Using the epochs assigned to the summands of (16) (say, a_i), one may analyze time-dependent correlations within $F_i(t)$. Clearly, the entire analysis can be repeated with the correlation (19) as a measure of trend similarity.

6 Discussion

The methods developed in this paper are based on the computational technique (see Section 2) for solving the linear interpolation problem for time series. This problem includes two principal difficulties. The first is a fundamental one: there is a tradeoff between the quality of a possible approximation and its detail. The second difficulty is purely computational: There are $(n-2)!/(n-1-k)!(k+1)!$ ways to construct a piecewise linear approximation with a given number k of segments and n observational epochs. Clearly, the search for the optimum over all possible approximations is unacceptable for operational use, and computationally effective algorithms are to be invented. Here we resolve the first difficulty by introducing the optimality criterion (3,4) of Section 2.2, and the second by replacing the original time series with its "skeleton" that includes only the edge points defined in Section 2.3. The whole analysis is then done hierarchically, in a multiscale self-similar fashion. This contributes to computational efficiency as well as to the imprecision of the final result, since the errors made in the first steps of the decomposition may affect all the consecutive steps. It would therefore be interesting to study a) deviations of the MTD approximations from the optimal (in a squared deviation sense) piecewise linear approximations with the same number of segments, and b) the history of the first-step errors.

The procedure for edge point detection is introduced here (Section 2.3) in its simplest (not to say most naive) form and is subject to further improvement. Nevertheless, even in its present form, the MTA has the potential to be an effective tool for solving a

wide spectrum of applied problems, ranging from exploratory data analysis to studying hierarchical scaling for time series.

Recently, several techniques based on properties of local linear trends were proposed and studied. The Detrended Fluctuation Analysis (DFA) [5] was shown to be a powerful tool for multiscale analysis and interpretation of diverse medical and financial data. Contrary to our analysis, DFA uses a predefined interval partition scheme independent of the particular series at hand. It is oriented toward analysis of variations, rather than the trend structure itself. An alternative approach to the problem of detection of local linear trends is discussed in [12].

The problem considered in this paper naturally extends to higher dimensions. However, it is not clear how to apply the ideas developed here even to 2D and this issue deserves special attention. Interestingly, elegant theoretical results on rectifiable curves by P. Jones [13] are tightly related to detection of linear structures in point clouds. Various methods of multiscale geometric analysis based on Jones' theory ([14] and references therein) use predefined (dyadic) partition schemes. It would be very important to find algorithms for fast linearization in point clouds.

It is worth mentioning that the self-affine analysis of Section 3 may be done equally effectively by a multitude of techniques, and MTA is by no means claimed to be the most efficient one. We include this section in order to demonstrate the diversity of possible applications based on the single decomposition (MTD) of a time series.

Acknowledgments This work was supported by a Collaborative Activity Award for Studying Complex Systems from the 21st Century Science Initiative of the James S. McDonnell Foundation.

A Mandelbrot cascade measures

A Mandelbrot cascade measure $M(r_i, m_i)$, $i = 1, \dots, n$ on the interval $[0, 1]$ is constructed as follows. At step 0 there is a unit mass distributed uniformly over the whole interval. At the first step we divide the interval $[0, 1]$ into n subintervals of lengths r_i , $\sum_{i=1}^n r_i = 1$ and assign to them masses m_i , $\sum_{i=1}^n m_i = 1$. Within each interval the mass distribution is uniform. Next, we divide each subinterval i into n subsubintervals and assign to them uniform masses $m_i \cdot m_j$, $j = 1, \dots, n$, and so on. Therefore, at the k th step the interval $[0, 1]$ is divided into n^k subintervals, each carrying the uniform mass $m_{i_1} \cdot \dots \cdot m_{i_k}$, with i_k taken from the set $1, \dots, n$ with possible repetitions.

Such measures were introduced first to model turbulent dissipation, and were studied by Mandelbrot [15].

Figure captions

Figure 8. Error-length dependence for individual vertices of trees M_X corresponding to FBW with $Ha = 0.1, 0.9$. The scaling (8) is clearly observed.

Figure 16. Correlation (reciprocal distance) μ (17) between MTD of two signals shown in Fig. 15 (panel a) and two independent Brownian walks (panel b).

Figure 18. Structure of the signals $F_i(t), i = 1, 2$ shown in Fig. 15. a),e) Original signals $F_i(t)$. b),f) Coupling parts $A_i(t) \cdot X(t)$. c),g) Non-linear deterministic trends. d),h) Random drifts.

Figure 19. Reconstruction (solid lines) of the coupling parts $A_i(t) \cdot X(t)$ (dashed lines). See Section 5.3.1 for discussion.

References

- [1] Sklansky, J., and V. Gonzalez, 1980. Fast polygonal approximation of digital curves, *Pattern Recognition*, **12**, 327-331.
- [2] Roberge J., 1985. A data reduction algorithm for plain curves, *Computer Vision, Graphics and Image Processing*, **29**, 168-195.
- [3] Natarajan, B. K., 1991. On piecewise linear approximations to curves, *SIAM Conference on Geometric Design*.
- [4] Turcotte, D.L., 1997. Fractals and Chaos in Geology and Geophysics. (2nd edition). Cambridge University Press. 398 pp.
- [5] Peng, C.-K., Havlin, S., Stanley, H.E., Goldberger, A.L., 1995. Quantification of scaling exponents and crossover phenomena in nonstationary heartbeat time series. *Chaos*, **5**, 82-87.
- [6] Horton, R.E., 1945. Erosional development of streams and their drainage basins: Hydrophysical approach to quantitative morphology, *Geol. Soc. Am. Bull.*, **56**, 275-370.
- [7] Strahler A. N., 1957. Quantitative analysis of watershed geomorphology. *Trans. Am. Geophys. Un.*, **38**, 913-920.
- [8] Badii, R., and Politi, A. 1997. *Complexity: Hierarchical Structures and Scaling in Physics*. Cambridge University Press. 318 pp.
- [9] Newman, W.I., Turcotte, D.L., and Gabrielov, A. 1997. Fractal trees with side branching. *Fractals*, **5**, 603-614
- [10] Gabrielov, A., Newman, W.I., and Turcotte, D.L. 1990. An exactly soluble hierarchical clustering model: inverse cascades, self-similarity, and scaling. *Phys. Rev. E*, **60**, 5293-5300.
- [11] Toroczkai, Z. 2001. Topological classification of the Horton-Strahler index on binary trees, *Phys. Rev. E*, **65**, 016130.
- [12] Cheung J. T-Y., and Stephanopoulos G. 1990. Representation of process trends. Part I. A formal representation framework. *Computer Chem. Eng.*, **14**, 495-510.
- [13] Jones, P.W., 1990. Rectifiable sets and traveling salesman problem. *Invent. Math.*, **102**(1):1-15.
- [14] Lerman, G., 2003. Quantifying curvelike structures of measures by using L_2 Jones quantities. To appear in *Communications on Pure and Applied Math.*

- [15] Mandelbrot, B. 1977. *Fractals: Form, Chance and Dimension*. Freeman & Co., San Francisco.

This figure "figure8.gif" is available in "gif" format from:

<http://arxiv.org/ps/physics/0305013v1>

This figure "figure16.gif" is available in "gif" format from:

<http://arxiv.org/ps/physics/0305013v1>

This figure "figure18.gif" is available in "gif" format from:

<http://arxiv.org/ps/physics/0305013v1>

This figure "figure19.gif" is available in "gif" format from:

<http://arxiv.org/ps/physics/0305013v1>